


Interactome INSIDER: a structural interactome browser for genomic studies

Michael J Meyer^{1-3,6}, Juan Felipe Beltrán^{1,2,6}, Siqi Liang^{1,2,6}, Robert Fragoza^{2,4}, Aaron Rumack^{1,2}, Jin Liang², Xiaomu Wei^{1,5} & Haiyuan Yu^{1,2} 

We present Interactome INSIDER, a tool to link genomic variant information with structural protein–protein interactomes. Underlying this tool is the application of machine learning to predict protein interaction interfaces for 185,957 protein interactions with previously unresolved interfaces in human and seven model organisms, including the entire experimentally determined human binary interactome. Predicted interfaces exhibit functional properties similar to those of known interfaces, including enrichment for disease mutations and recurrent cancer mutations. Through 2,164 *de novo* mutagenesis experiments, we show that mutations of predicted and known interface residues disrupt interactions at a similar rate and much more frequently than mutations outside of predicted interfaces. To spur functional genomic studies, Interactome INSIDER (<http://interactomeinsider.yulab.org>) enables users to identify whether variants or disease mutations are enriched in known and predicted interaction interfaces at various resolutions. Users may explore known population variants, disease mutations, and somatic cancer mutations, or they may upload their own set of mutations for this purpose.

Protein–protein interactions facilitate much of known cellular function. Recent efforts to experimentally determine protein interactomes in human¹ and model organisms^{2–4}, in addition to literature curation of small-scale interaction assays⁵, have dramatically increased the scale of known interactome networks. Studies of these interactomes have allowed researchers to elucidate how modes of evolution affect the functional fates of paralogs⁴ and to examine, on a genomic scale, network interconnectivities that determine cellular functions and disease states⁶.

While simply knowing which proteins interact with each other provides valuable information to spur functional studies, far more specific hypotheses can be tested if the spatial contacts of interacting proteins are known⁷. In the study of human disease, it has

been demonstrated that mutations tend to localize to interaction interfaces, and mutations on the same protein may cause clinically distinct diseases by disrupting interactions with different partners^{6,8}. However, the binding topologies of interacting proteins can only be determined at atomic resolution through X-ray crystallography, NMR, and (more recently) cryo-EM⁹ experiments, which limits the number of interactions with resolved interaction interfaces.

To study protein function on a genomic scale, especially as it relates to human disease, a large-scale set of protein interaction interfaces is needed. Thus far, computational methods such as docking¹⁰ and homology modeling¹¹ have been employed to predict the atomic-level bound conformations of interactions whose experimental structures have not yet been determined. However, docked models are not yet available on a large scale; and while homology modeling has been used to produce models at scale¹², it is only amenable to interactions with structural templates (<5% of known interactions). Together, cocrystal structures and homology models comprise the currently available precalculated sources of structural interactomes, covering only ~6% of all known interactions (Fig. 1a,b).

Here, we present Interactome INSIDER (integrated structural interactome and genomic data browser), a tool for functional exploration of human disease on a genomic scale (<http://interactomeinsider.yulab.org>). Interactome INSIDER is based on a structurally resolved, proteome-wide human interactome. We assembled this resource by building an interactome-wide set of protein interaction interfaces at the highest resolution possible for each interaction. We compiled structural interactomes by calculating interfaces in experimental cocrystal structures and homology models, when available. For the remaining ~94% of interactions, we applied a machine-learning framework to predict partner-specific interfaces by applying recent advances in coevolution- and docking-based feature construction^{13,14}. Interactome INSIDER combines predicted interaction interfaces for 185,957 previously unresolved interactions (including the full human

¹Department of Biological Statistics and Computational Biology, Cornell University, Ithaca, New York, USA. ²Weill Institute for Cell and Molecular Biology, Cornell University, Ithaca, New York, USA. ³Tri-Institutional Training Program in Computational Biology and Medicine, New York, New York, USA. ⁴Department of Molecular Biology and Genetics, Cornell University, Ithaca, New York, USA. ⁵Department of Medicine, Weill Cornell College of Medicine, New York, New York, USA. ⁶These authors contributed equally to this work. Correspondence should be addressed to H.Y. (haiyuan.yu@cornell.edu).

RECEIVED 24 JANUARY; ACCEPTED 22 OCTOBER; PUBLISHED ONLINE 1 JANUARY 2018; DOI:10.1038/NMETH.4540

interactome and seven commonly studied model organisms) with disease mutations and functional annotations in an interactive toolbox designed to spur functional genomics research. It allows users to find enrichment of disease mutations at different scales: in protein interaction domains, in residues, and through atomic 3D clustering in protein interfaces.

RESULTS

To build Interactome INSIDER, we first constructed an interactome-wide set of protein interaction interfaces. While there are well-established methods for predicting whether two proteins interact^{15,16}, we focused on interactions that have been experimentally determined, but whose interfaces are unknown (**Supplementary Note 1**). For this task, there is a rich literature exploring the potential of many structural, evolutionary, and docking-based methods to predict protein interaction interfaces. However, so far none of these methods have been used to produce a whole-interactome data set of protein interaction interfaces (**Supplementary Note 2**).

We used ECLAIR (ensemble classifier learning algorithm to predict interface residues), a unified machine-learning framework, to predict the interfaces of protein interactions. ECLAIR leverages several complementary and proven classification features, including sequence-based biophysical features, structural features, and recently proposed features for predicting binding partner-specific interfaces, including coevolutionary^{17,18} and docking-based metrics¹⁴ (**Supplementary Note 3; Supplementary Figs. 1 and 2**). Unfortunately, many protein–protein interactions have missing features (especially structural features). In fact, this type of nonrandom missing-feature problem is present in many biological prediction studies and cannot be adequately resolved by commonly used imputation methods. To address this issue, ECLAIR is structured as an ensemble of eight independent classifiers, each of which covers a common case of feature availability. This unique structure of ECLAIR enables it to be applied to any interaction while using the most informative subset of available features for that interaction (**Supplementary Notes 4 and 5; Supplementary Figs. 3 and 4**).

We comprehensively optimized hyperparameters for ECLAIR using a recently published Bayesian method, the tree-structured Parzen estimator approach (TPE)¹⁹, which allowed us to simultaneously tune up to eight hyperparameters for each subclassifier. We trained and tested each ECLAIR subclassifier using a set of known protein interaction interfaces, and we observed that interfaces can be predicted by the single, top-performing subclassifier available for each residue. Subclassifier performance increases with the number of features used. We observe an area under the ROC curve (AUROC) of 0.64 for our top-sequence-only subclassifier and AUROC of 0.80 for our top subclassifier using both sequence and structural features. In total, we used ECLAIR to predict the interfaces of 185,957 interactions with previously unknown interfaces, including for 115,576 human interactions (**Supplementary Fig. 5**). Specifically, residues classified by ECLAIR with a high or very high interface potential have a precision of 0.69, and >90% of all 115,576 human interactions with predicted interfaces in Interactome INSIDER have one or more residues that fall into these categories. We supplemented known structural interfaces from cocrystallized proteins and homology models with our predictions to create structural interactomes at both the atomic and residue levels (**Fig. 2a**) in

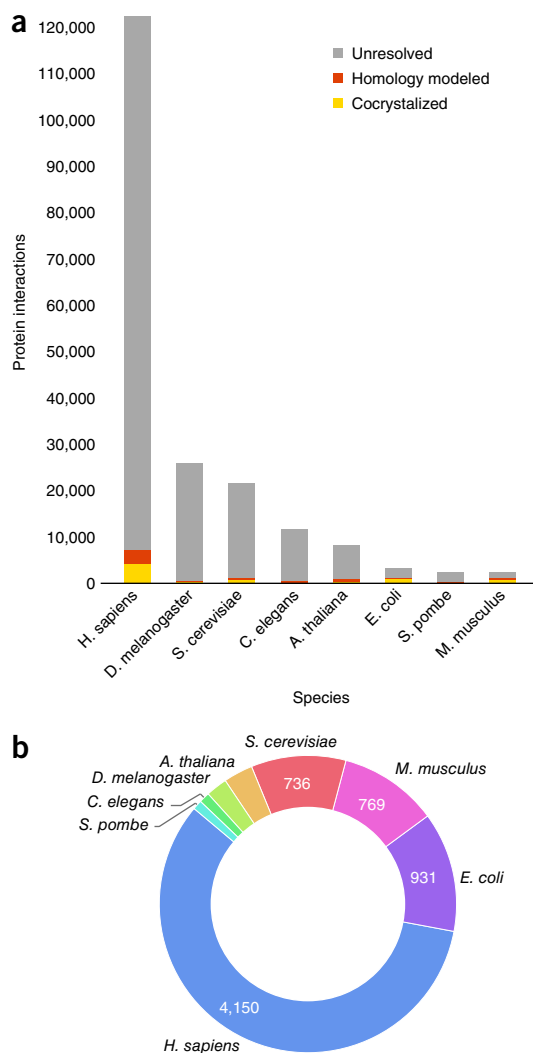


Figure 1 | The current size of structural interactomes. **(a)** The plot shows the coverage (number of protein interactions) of known high-quality binary interactomes with precomputed cocomplexed protein structures. **(b)** The number of interactions from the eight largest interactomes with experimentally solved structures.

seven model organisms and human (including all 122,647 human experimentally determined binary interactions reported in major databases; see Online Methods).

Comprehensive evaluation of predicted interfaces

We established that our predictions are of high quality through both machine learning and biological evaluation. We first evaluated the trade-offs between false-positive rate and true-positive rate and between precision and recall for each of the eight independent subclassifiers that compose ECLAIR. As expected, we find that as more informative features are added to subsequent classifiers, the areas under the ROC and precision–recall curves increase, and this justifies the use of classifiers trained on more features for residues where this information is available (**Supplementary Fig. 6**).

We next compared ECLAIR with several other prediction methods through two independent validations. First, we used several readily available predictors^{20–24} to predict interfaces for

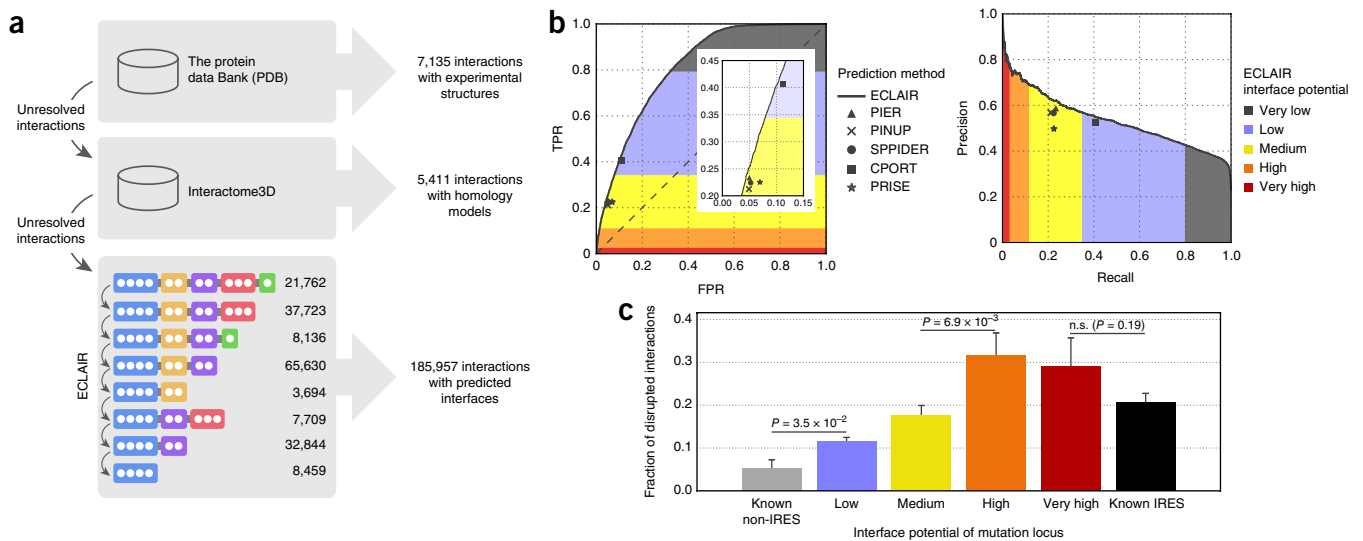


Figure 2 | ECLAIR prediction results. **(a)** Workflow for classifying interfaces for all interactions in eight species. Interactions without experimentally determined or homology-modeled interfaces are classified by ECLAIR. **(b)** ROC and precision–recall curves comparing ECLAIR with the indicated interface residue prediction methods. **(c)** Fraction of interactions disrupted by the introduction of random population variants in known and predicted interfaces. (Significance determined by two-sided Z-test; n.s., not significant.)

interactions in our testing set. We found that for the set of interactions for which all classifiers can predict, ECLAIR performs as well or slightly better than these methods by measures of precision, recall, true-positive rate and false-positive rate (**Fig. 2b** and **Supplementary Fig. 7**). Finally, we applied ECLAIR to a standard external benchmark set of protein interaction interfaces²⁵ which has been used to evaluate the performance of ten other interface prediction methods²⁶. We found that ECLAIR outperforms all benchmarked methods in accuracy and is comparable to the top performers in all other metrics (**Supplementary Table 1**). Furthermore, ECLAIR is applicable to any interaction, while methods in this benchmark rely on single-protein-structure inputs, which makes them much less applicable to genome-wide studies. In fact, 86.1% of interactions without structural features contain at least one predicted interface residue at an ECLAIR score corresponding to a precision ≥ 0.6 .

We also performed $>2,000$ mutagenesis experiments to measure the rate at which population variants in our predicted interfaces disrupt interactions in comparison to variants within known cocrystal interfaces and noninterfaces (see Online Methods). Using our high-throughput yeast-two-hybrid assay²⁷, we found that mutations in our predicted interfaces break their corresponding interactions at a significantly higher rate than those known to be away from the interface ($P < 0.035$) and at similar rates to mutations in known interfaces. Since it is known that mutations at protein interfaces are more likely to break interactions^{6,27}, our experimental results indicate that there is rich functional signal in our ECLAIR predictions (**Fig. 2c**).

Functional annotation of disease mutations in structural interactomes

Interactome INSIDER is a tool for identifying functionally enriched areas of protein interactomes and for browsing our multiscale structural interactome networks—198,503 protein interactions whose interfaces have been either experimentally

determined, homology modeled, or predicted using ECLAIR. Interactome INSIDER also includes 56,159 disease mutations from HGMD²⁸ and ClinVar²⁹ and 1,300,352 somatic cancer mutations from COSMIC³⁰ with their per-disease, precalculated enrichment in protein interaction interfaces at the residue level, domain level, and through atomic clustering. The site includes information on $>600,000$ population variants from the Exome Sequencing Project³¹, 1000 Genomes Project³², and more³³ (see Online Methods). Users can search Interactome INSIDER by protein to retrieve all interaction partners and their interfaces, or they can search by disease to retrieve all interaction interfaces that are enriched for mutations of that disease. Additionally, users can upload their own set of mutations to find how they are distributed in the interactome and whether they are enriched in any protein interaction interfaces at the residue, domain, and atomic levels (**Fig. 3**).

We demonstrate the utility of Interactome INSIDER and the validity of its underlying database by investigating the functional and biological properties of our predicted interaction interfaces. We measured functional properties of our *in silico* predicted interfaces (those without prior experimental evidence) and compared these measurements to those of known interfaces from cocrystal structures. We found that disease mutations preferentially occur in our predicted interfaces at similar rates to those of known interface residues in PDB cocrystal structures (**Fig. 4a**), which indicates the viability of using predicted interfaces to study molecular disease mechanisms. Furthermore, each higher confidence bin of predicted interface residues is more likely to contain disease mutations than the previous, which shows that ECLAIR prediction scores are correlated with true protein function. We looked at the locations of somatic cancer mutations from COSMIC in our interface-resolved human interactome. We specifically focused on recurrent cancer mutations, as these are known to be more likely to be functional drivers^{34,35}. We found a marked enrichment of recurrent cancer mutations in our predicted interfaces

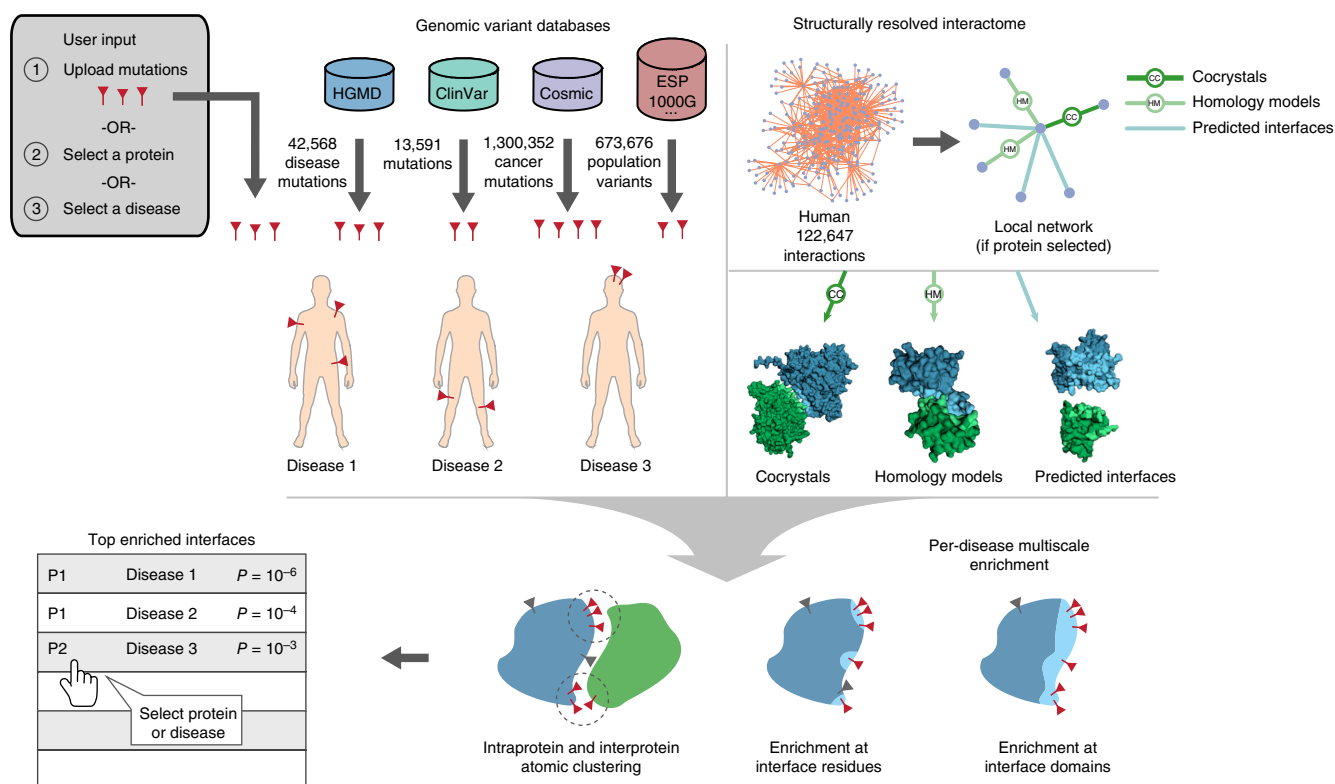


Figure 3 | Workflow for calculating mutation and variant enrichment using Interactome INSIDER (<http://interactomeinsider.yulab.org>). Users may submit mutations or select sets of known disease and cancer mutations to assess their enrichment in interface domains and residues, or they may compute 3D atomic clusters of mutations in proteins and across interfaces.

compared to outside these interfaces (Fig. 4b). The same trend is observed inside and outside of known interfaces from cocrystal structures, which suggests that the functional links between cancer and the potential disruption of protein interactions can be observed within the entire Interactome INSIDER human interface data set. We also looked at the distribution of population variants and show that their placement in and out of predicted interfaces matches that of known interfaces, with rarer mutations showing an enrichment in protein interfaces (Fig. 4c). Furthermore, population variants in our predicted interfaces are more likely to be damaging to protein function than variants outside of predicted interfaces, as predicted by PolyPhen-2 (ref. 36) (Fig. 4d) and EVmutation³⁷ (Fig. 4e), matching the established trend for experimentally determined interfaces³⁸. We validated many of these biological trends for interactions lacking structural features (Supplementary Figs. 8–10 and Supplementary Note 6), and this suggests the utility of Interactome INSIDER even in feature-poor interactions and across different resolution scales.

We used Interactome INSIDER to search for subnetworks in the human interactome that are enriched for mutations associated with a single disease by calculating the enrichment of disease mutations in interaction interfaces interactome wide. This identified the TGF- β /BMP signaling pathway, which is known to be involved in juvenile polyposis syndrome (JPS)³⁹ and contains multiple proteins harboring JPS mutations (Fig. 5a). We focused on a specific group of mutations in the SMAD4–SMAD8 interface, which can be found using 3D atomic clustering. Using our mutagenesis Y2H assay, we were able to test a JPS mutation (SMAD4 Y353S)⁴⁰, which is at the

interface of SMAD4–SMAD8, and show that it breaks this interaction, implicating SMAD8 in JPS (Fig. 5a and Supplementary Fig. 11). Although SMAD8 (also known as SMAD9) has not been reported to harbor JPS mutations in HGMD²⁸, its involvement in the disease has been suggested⁴¹, and this shows the ability of Interactome INSIDER to implicate new proteins in disease. Y353S is not predicted by ECLAIR to be at the interface of SMAD4 and another of its binding partners, RASSF5. Indeed, through our Y2H experiment, Y353S does not break this interaction, demonstrating the functional insight Interactome INSIDER can provide about differential interfaces and how they might be relevant to understanding the molecular mechanisms of disease.

Disease etiology revealed by partner-specific interfaces

Interactome INSIDER enables interrogation of different interfaces for the same protein, dependent upon its binding partner (Fig. 5b). For the study of protein function and disease, this is especially important, as a protein may maintain different functional pathways through different interfaces, and disruption of one interface may leave others intact^{4,8}. To test this on a large scale, we looked at pairs of disease mutations in the human interactome that appear at interaction interfaces, as predicted by ECLAIR. Similar to previous reports⁸, we observed that mutation pairs in the interface of two interacting proteins are much more likely to cause the same disease than mutation pairs in other interfaces of the same proteins that do not mediate the given interaction (Fig. 5c). We also find that mutation pairs on the same protein, but in separate interfaces with different binding partners, tend to cause

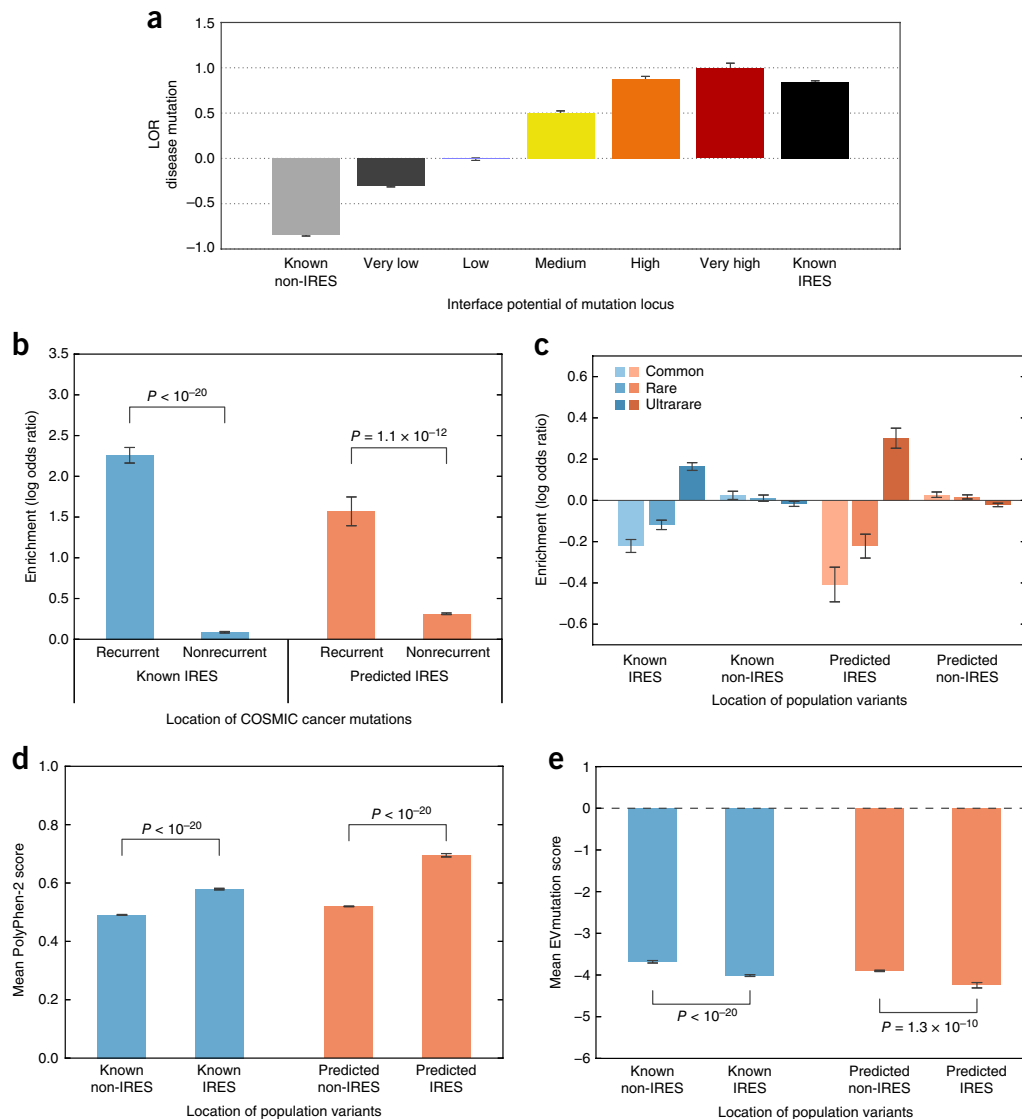


Figure 4 | Functional properties of predicted interfaces. **(a)** Enrichment of disease mutations in predicted and known interfaces. In **a–c**, enrichment (log odds ratio) is the odds of mutations and variants to appear inside and outside of predicted and known interfaces compared to the odds of any residues to exist in these categories. **(b)** Enrichment of recurrent cancer mutations in predicted and known interfaces. **(c)** Enrichment of rare and common population variants in predicted and known interfaces. **(d,e)** Predicted deleteriousness of population variants in known and predicted interfaces using PolyPhen-2 **(d)** or EVmutation **(e)**. (In **b**, significance determined by two-sided Z-test. In **d** and **e**, significance determined by a two-sided U-test. IRES, interface residues.)

different diseases (**Fig. 5d**). This trend is observed in both known and predicted interfaces. These results indicate that Interactome INSIDER can be used to form functional hypotheses about the specificity of mutations to specific interactions and molecular pathways.

We next used Interactome INSIDER to find subnetworks in the human interactome enriched for mutations associated with a single disease. We uncovered a set of interacting proteins known to harbor mutations causal for hypertrophic cardiomyopathy (HCM)⁴² and thereby recapitulated the core constituents of a known KEGG pathway related to the same disease (**Fig. 6**). These proteins were identified by enrichment of disease mutations in their shared interaction interfaces and, in the case of TNNT1–TNNC1, using cross-interface atomic clustering of disease mutation positions in 3D (features available via the Interactome INSIDER website). In addition to identifying known members of the HCM pathway,

Interactome INSIDER also identified several additional proteins, including CSRP3, MYOM1, ANKRD, and TCAP, which are not part of the known KEGG pathway but carry HCM mutations enriched at their respective interaction interfaces with members of the pathway. We also identified a protein, TNNT1, which, although it contains no HCM mutations of its own, can be implicated in HCM through its interactions with the two proteins TPM1 and TNNC1, which are enriched for HCM mutations at their interfaces with TNNT1. Finally, we note that Interactome INSIDER reveals cases of partner-specific interfaces in this pathway. For instance, the known HCM pathway protein TTN’s interface with ACTA1 is enriched for HCM mutations, and ACTA1 mutations are increasingly linked to HCM⁴³. On the other hand, a separate interface of ACTA1 with its binding partner dystrophin is enriched with mutations causing a distinct disorder, actin myopathy⁴⁴. This

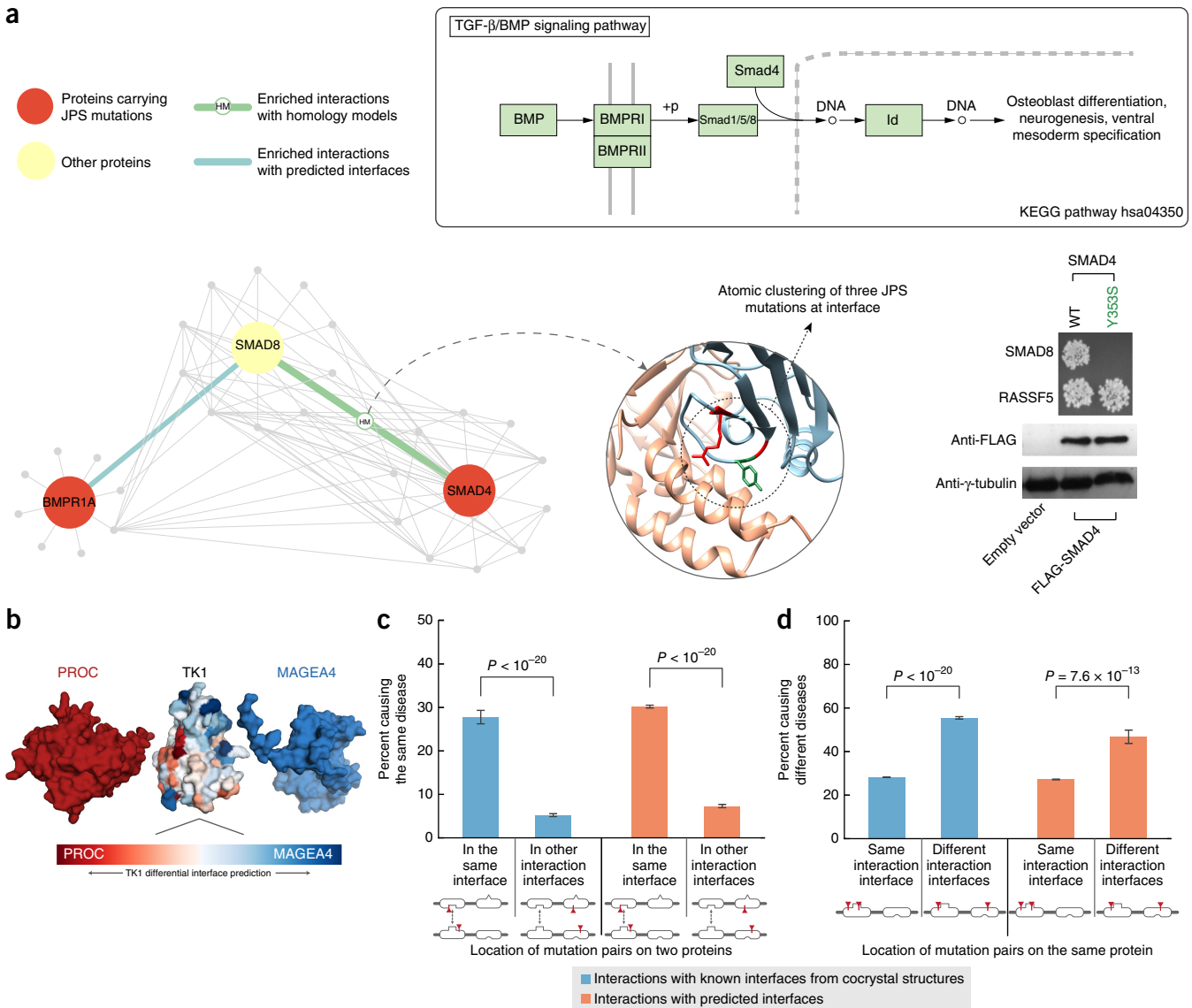


Figure 5 | Interaction-partner-specific interface prediction. (a) The top schematic depicts the TGF-β/BMP signaling pathway. The bottom schematic illustrates that atomic clustering reveals a mutation hotspot for juvenile polyposis syndrome at the interface of SMAD8 and SMAD4. At right, yeast-two-hybrid experiments test the interactions of one of the SMAD4 mutations (Y353S) with SMAD8 and RASSF5. The mutation is not predicted by ECLAIR to be at the SMAD4-RASSF5 interface. (b) Superimposed docking results of two different interaction partners with TK1. The differentially predicted interfaces of TK1 with each of its partners correspond with the orientation of the docked poses. (c) The plot shows the fraction of disease mutation pairs in known (blue) or predicted (orange) interfaces that cause the same disease when mutations are on either side of an interaction interface (in different proteins) compared to in other interaction interfaces (that don't facilitate the given interaction). (d) The plot shows the fraction of disease mutation pairs in known (blue) or predicted (orange) interfaces that cause different diseases when mutations are in the same interaction interface compared to in different interaction interfaces (interaction with other proteins is not shown). (Significance determined by two-sided Z-test.)

shows how ACTA1 can play roles in two different diseases through separate interaction interfaces with TTN and dystrophin and demonstrates Interactome INSIDER's unique ability to discover such cases of differential function mirroring differential interfaces.

DISCUSSION

We anticipate Interactome INSIDER will help bridge the divide between genomic-scale data sets and structural proteomic analyses. Now that large-scale sequencing data from many contexts are readily available, for instance from whole-genome and whole-exome population variant studies^{31,45} and cancer studies^{46,47},

researchers have become increasingly interested in ways to assess the potential functional consequences of variants on a genomic scale^{48,49}. Recently, we and others have developed methods to predict functional cancer driver mutations by finding hotspots of mutations in the structural proteome^{35,50}. With the comprehensive map of protein interfaces presented, we can now go a step further to predict specific etiologies of cancer and disease based on induced biophysical effects^{51,52} that may break interactions. Because our interface map is partner specific, it can also be applied to predict pleiotropic effects, wherein several mutations in a single protein may affect different pathways depending upon

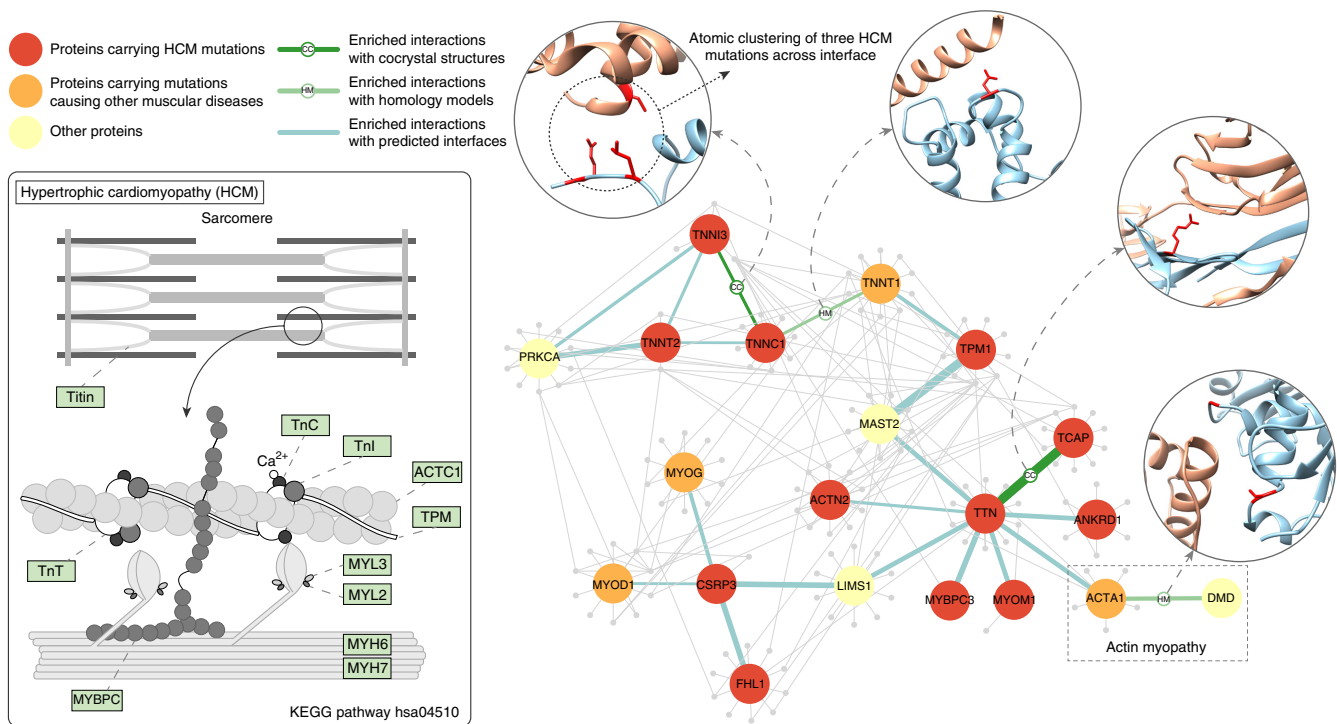


Figure 6 | The hypertrophic cardiomyopathy (HCM) pathway. The schematic on the left shows the interaction of proteins in the HCM KEGG pathway (hsa04510). On the right is shown a network of KEGG pathway proteins and their structurally resolved interactions from Interactome INSIDER. Proteins that harbor HCM mutations are colored in red. Interfaces are noted for their enrichment of HCM mutations.

which binding interfaces are mutated⁸. This could be the basis for designing new therapeutics and for rational drug design to selectively target specific protein functional sites⁵³.

We have shown that hyperparameter optimization, which is surprisingly lacking in much of the current literature, can drastically improve the performance of classifiers for biological classification studies. The tiered ensemble form of the ECLAIR classifier represents a broadly applicable paradigm in practical machine learning that could be readily applied to solving other problems with large amounts of nonuniformly missing data, which very frequently occur in biology on account of study biases.

With future increases to the scale of biological databases from which we derive features, we expect that Interactome INSIDER will come to encompass even higher confidence predictions for many more interactions, thereby becoming increasingly applicable to functional studies. This may also address some limitations of structural databases today. For instance, the PDB is depleted of disordered proteins⁵⁴, and it has been shown that disordered regions can form interfaces⁵⁵. Since ECLAIR has not been trained on disordered interfaces, it is unlikely to predict new disordered interfaces. However, the ensemble classifier structure of ECLAIR uniquely positions it to incorporate all newly available evidence into interface predictions without sacrificing quality or scale, and this ensures a high-quality map of interaction interfaces now and in the future. Furthermore, the addition of new variants, especially cancer mutations and population variants from large-scale sequencing studies, will only increase the value of performing systems-level explorations with Interactome INSIDER.

METHODS

Methods, including statements of data availability and any associated accession codes and references, are available in the [online version of the paper](#).

Note: Any Supplementary Information and Source Data files are available in the online version of the paper.

ACKNOWLEDGMENTS

The authors would like to thank G. Hooker, D. Bindel, and K. Weinberger for helpful discussions and J. VanEe for technical support. This work was supported by National Institute of General Medical Sciences grants (R01 GM097358, R01 GM104424, R01 GM124559); National Cancer Institute grant (R01 CA167824); Eunice Kennedy Shriver National Institute of Child Health and Human Development grant (R01 HD082568); National Human Genome Research Institute grant (UM1 HG009393); National Science Foundation grant (DBI-1661380); and Simons Foundation Autism Research Initiative grant (367561) to H.Y.

AUTHOR CONTRIBUTIONS

M.J.M., J.F.B., S.L., and H.Y. conceived the study. H.Y. oversaw all aspects of the study. M.J.M., J.F.B., S.L., and A.R. performed computational analyses. M.J.M. and J.F.B. designed ECLAIR. J.F.B. designed the web interface. R.F., J.L., and X.W. performed laboratory experiments. M.J.M. wrote the manuscript with input from J.F.B., S.L., and H.Y. All authors edited and approved of the final manuscript.

COMPETING FINANCIAL INTERESTS

The authors declare no competing financial interests.

Reprints and permissions information is available online at <http://www.nature.com/reprints/index.html>. **Publisher's note: Springer Nature remains neutral with regard to jurisdictional claims in published maps and institutional affiliations.**

1. Rolland, T. *et al.* A proteome-scale map of the human interactome network. *Cell* **159**, 1212–1226 (2014).

2. Arabidopsis Interactome Mapping Consortium. Evidence for network evolution in an *Arabidopsis* interactome map. *Science* **333**, 601–607 (2011).
3. Yu, H. *et al.* High-quality binary protein interaction map of the yeast interactome network. *Science* **322**, 104–110 (2008).
4. Vo, T.V. *et al.* A proteome-wide fission yeast interactome reveals network evolution principles from yeasts to human. *Cell* **164**, 310–323 (2016).
5. Das, J. & Yu, H. HINT: High-quality protein interactomes and their applications in understanding human disease. *BMC Syst. Biol.* **6**, 92 (2012).
6. Sahni, N. *et al.* Widespread macromolecular interaction perturbations in human genetic disorders. *Cell* **161**, 647–660 (2015).
7. Kim, P.M., Lu, L.J., Xia, Y. & Gerstein, M.B. Relating three-dimensional structures to protein networks provides evolutionary insights. *Science* **314**, 1938–1941 (2006).
8. Wang, X. *et al.* Three-dimensional reconstruction of protein networks provides insight into human genetic disease. *Nat. Biotechnol.* **30**, 159–164 (2012).
9. Kühlbrandt, W. Cryo-EM enters a new era. *eLife* **3**, e03678 (2014).
10. Halperin, I., Ma, B., Wolfson, H. & Nussinov, R. Principles of docking: an overview of search algorithms and a guide to scoring functions. *Proteins* **47**, 409–443 (2002).
11. Šali, A. & Blundell, T.L. Comparative protein modelling by satisfaction of spatial restraints. *J. Mol. Biol.* **234**, 779–815 (1993).
12. Mosca, R., Céol, A. & Aloy, P. Interactome3D: adding structural details to protein networks. *Nat. Methods* **10**, 47–53 (2013).
13. Hopf, T.A. *et al.* Sequence co-evolution gives 3D contacts and structures of protein complexes. *eLife* **3**, 03430 (2014).
14. Hwang, H., Vreven, T. & Weng, Z. Binding interface prediction by combining protein-protein docking results. *Proteins* **82**, 57–66 (2014).
15. Zhang, Q.C. *et al.* Structure-based prediction of protein-protein interactions on a genome-wide scale. *Nature* **490**, 556–560 (2012).
16. Garzón, J.I. *et al.* A computational interactome and functional annotation for the human proteome. *eLife* **5**, 18715 (2016).
17. Morcos, F. *et al.* Direct-coupling analysis of residue coevolution captures native contacts across many protein families. *Proc. Natl. Acad. Sci. USA* **108**, E1293–E1301 (2011).
18. Lockless, S.W. & Ranganathan, R. Evolutionarily conserved pathways of energetic connectivity in protein families. *Science* **286**, 295–299 (1999).
19. Bergstra, J.S., Bardenet, R., Bengio, Y. & Kégl, B. Algorithms for hyperparameter optimization. In *Advances in Neural Information Processing Systems* (eds. Shawe-Taylor, T *et al.*) 2546–2554 (NIPS, 2011).
20. Kufareva, I., Budagyan, L., Raush, E., Totrov, M. & Abagyan, R. PIER: protein interface recognition for structural proteomics. *Proteins* **67**, 400–417 (2007).
21. Liang, S., Zhang, C., Liu, S. & Zhou, Y. Protein binding site prediction using an empirical scoring function. *Nucleic Acids Res.* **34**, 3698–3707 (2006).
22. Porollo, A. & Meller, J. Prediction-based fingerprints of protein-protein interactions. *Proteins* **66**, 630–645 (2007).
23. de Vries, S.J. & Bonvin, A.M. CPORT: a consensus interface predictor and its performance in prediction-driven docking with HADDOCK. *PLoS One* **6**, e17695 (2011).
24. Jordan, R.A., El-Manzalawy, Y., Dobbs, D. & Honavar, V. Predicting protein-protein interface residues using local surface structural similarity. *BMC Bioinformatics* **13**, 41 (2012).
25. Hwang, H., Vreven, T., Janin, J. & Weng, Z. Protein-protein docking benchmark version 4.0. *Proteins* **78**, 3111–3114 (2010).
26. Maheshwari, S. & Brylinski, M. Predicting protein interface residues using easily accessible on-line resources. *Brief. Bioinform.* **16**, 1025–1034 (2015).
27. Wei, X. *et al.* A massively parallel pipeline to clone DNA variants and examine molecular phenotypes of human disease mutations. *PLoS Genet.* **10**, e1004819 (2014).
28. Stenson, P.D. *et al.* The Human Gene Mutation Database: building a comprehensive mutation repository for clinical and molecular genetics, diagnostic testing and personalized genomic medicine. *Hum. Genet.* **133**, 1–9 (2014).
29. Landrum, M.J. *et al.* ClinVar: public archive of interpretations of clinically relevant variants. *Nucleic Acids Res.* **44**, D862–D868 (2016).
30. Forbes, S.A. *et al.* COSMIC: exploring the world’s knowledge of somatic mutations in human cancer. *Nucleic Acids Res.* **43**, D805–D811 (2015).
31. Fu, W. *et al.* Analysis of 6,515 exomes reveals the recent origin of most human protein-coding variants. *Nature* **493**, 216–220 (2013).
32. 1000 Genomes Project Consortium *et al.* A global reference for human genetic variation. *Nature* **526**, 68–74 (2015).
33. UniProt Consortium. UniProt: a hub for protein information. *Nucleic Acids Res.* **43**, D204–D212 (2015).
34. Hodis, E. *et al.* A landscape of driver mutations in melanoma. *Cell* **150**, 251–263 (2012).
35. Meyer, M.J. *et al.* mutation3D: cancer gene prediction through atomic clustering of coding variants in the structural proteome. *Hum. Mutat.* **37**, 447–456 (2016).
36. Adzhubei, I.A. *et al.* A method and server for predicting damaging missense mutations. *Nat. Methods* **7**, 248–249 (2010).
37. Hopf, T.A. *et al.* Mutation effects predicted from sequence co-variation. *Nat. Biotechnol.* **35**, 128–135 (2017).
38. David, A., Razali, R., Wass, M.N. & Sternberg, M.J. Protein-protein interaction sites are hot spots for disease-associated nonsynonymous SNPs. *Hum. Mutat.* **33**, 359–363 (2012).
39. Wang, R.N. *et al.* Bone Morphogenetic Protein (BMP) signaling in development and human diseases. *Genes Dis.* **1**, 87–105 (2014).
40. Roth, S. *et al.* SMAD genes in juvenile polyposis. *Genes Chromosom. Cancer* **26**, 54–61 (1999).
41. Ngeow, J. *et al.* Exome sequencing reveals germline *SMAD9* mutation that reduces phosphatase and tensin homolog expression and is associated with hamartomatous polyposis and gastrointestinal ganglioneuromas. *Gastroenterology* **149**, 886–889 e5 (2015).
42. Maron, B.J. Hypertrophic cardiomyopathy: a systematic review. *J. Am. Med. Assoc.* **287**, 1308–1320 (2002).
43. Donkervoort, S. *et al.* Cardiomyopathy in patients with *ACTA1*-myopathy. *Neuromuscul. Disord.* **25**, S287 (2015).
44. Sparrow, J.C. *et al.* Muscle disease caused by mutations in the skeletal muscle alpha-actin gene (*ACTA1*). *Neuromuscul. Disord.* **13**, 519–531 (2003).
45. Lek, M. *et al.* Analysis of protein-coding genetic variation in 60,706 humans. *Nature* **536**, 285–291 (2016).
46. Forbes, S.A. *et al.* COSMIC: mining complete cancer genomes in the Catalogue of Somatic Mutations in Cancer. *Nucleic Acids Res.* **39**, D945–D950 (2011).
47. Kandath, C. *et al.* Mutational landscape and significance across 12 major cancer types. *Nature* **502**, 333–339 (2013).
48. Lawrence, M.S. *et al.* Mutational heterogeneity in cancer and the search for new cancer-associated genes. *Nature* **499**, 214–218 (2013).
49. Taşan, M. *et al.* Selecting causal genes from genome-wide association studies via functionally coherent subnetworks. *Nat. Methods* **12**, 154–159 (2015).
50. Kamburov, A. *et al.* Comprehensive assessment of cancer missense mutation clustering in protein structures. *Proc. Natl. Acad. Sci. USA* **112**, E5486–E5495 (2015).
51. Kucukkal, T.G., Petukh, M., Li, L. & Alexov, E. Structural and physico-chemical effects of disease and non-disease nsSNPs on proteins. *Curr. Opin. Struct. Biol.* **32**, 18–24 (2015).
52. Li, M., Petukh, M., Alexov, E. & Panchenko, A.R. Predicting the impact of missense mutations on protein-protein binding affinity. *J. Chem. Theory Comput.* **10**, 1770–1780 (2014).
53. Lounnas, V. *et al.* Current progress in structure-based rational drug design marks a new mindset in drug discovery. *Comput. Struct. Biotechnol. J.* **5**, e201302011 (2013).
54. Peng, K., Obradovic, Z. & Vucetic, S. Exploring bias in the Protein Data Bank using contrast classifiers. *Pac. Symp. Biocomput.* **2004**, 435–446 (2004).
55. Dunker, A.K. *et al.* The unfoldomics decade: an update on intrinsically disordered proteins. *BMC Genomics* **9**, S1 (2008).

ONLINE METHODS

Interaction data sets. We compiled binary protein interactions available for *H. sapiens*, *D. melanogaster*, *S. cerevisiae*, *C. elegans*, *A. thaliana*, *E. coli*, *S. pombe*, and *M. musculus* from seven primary interaction databases. These databases include IMEx⁵⁶ partners DIP⁵⁷, IntAct⁵⁸, and MINT⁵⁹; IMEx observer BioGRID⁶⁰; and additional sources iRefWeb⁶¹, HPRD⁶², and MIPS⁶³. Furthermore, iRefWeb combines interaction data from BIND⁶⁴, CORUM⁶⁵, MPact⁶⁶, OPHID⁶⁷, and MPPI⁶⁸. We filtered these interactions using the PSI-MI⁶⁹ evidence codes of assays that can determine experimental binary interactions (**Supplementary Table 2**), as these are interactions where proteins are known to share a direct-binding interface that we can then predict⁵. In total, we curated 198,503 interactions in these eight species, including the full experimentally determined binary interactome in human (122,647 interactions) (**Supplementary Note 1**). Those interactions with known interface residues based on available cocrystal structures in the Protein Data Bank (PDB)⁷⁰ were set aside for use in training and testing the classifier. Interactions without known interface residues comprise the set for which we make predictions.

Testing and training sets for interface residue prediction. For those interactions with known cocrystal structures in the PDB, we calculate interface residues for their specific binding partners. To identify UniProt protein sequences in the PDB, we use SIFTS⁷¹, which provides a mapping of PDB-indexed residues to UniProt-indexed residues³³. For each interaction and representative cocrystal structure, interface residues are calculated by assessing the change in solvent-accessible surface area of the proteins in complex and apart using NACCESS⁷². Any residue that is at the surface of a protein ($\geq 15\%$ exposed surface) and whose solvent-accessible surface area (SASA) decreases by $\geq 1.0 \text{ \AA}^2$ in complex is considered to be at the interface. We aggregate interface residues across all available structures in the PDB for a given interaction, wherein a residue is considered to be at the interface of the interaction if it has been calculated to be at the interface in one or more cocrystal structures of that interaction (all other residues are considered to be away from the interface). In building our final training and testing sets, we only consider interactions for which aggregated cocrystal structures have combined to cover at least 50% of UniProt residues for both interacting proteins.

The training and testing sets each include a random selection of 400 interactions with known cocrystal structures, of which 200 are heterodimers and 200 are homodimers (**Supplementary Table 3**). To ensure an unbiased performance evaluation, we disallowed any homologous interactions (i.e., interactions whose structures could be used as templates for homology modeling) between the training and testing set. We also disallowed repeated proteins between the two sets to avoid simply reporting a remembered shared interface between a protein and multiple binding partners.

Hyperparameter optimization with TPE. To train our ensemble of classifiers that comprise ECLAIR, we used the tree-structured Parzen estimator approach (TPE)¹⁹, a Bayesian method for optimizing hyperparameters for machine learning algorithms. TPE models the probability distribution $p(x|y)$ of hyperparameters

given evaluated loss from a defined objective function, $L(x)$. We selected the following loss function to minimize based on classical hyperparameter inputs and residue window sizes:

$$L(\theta, w) = 1 - \min_{n \in \{1, 2, 3\}} \{AUROC_{\theta, w, n}\}$$

where x is comprised of θ , a set of hyperparameters, and w , a set of residue window sizes. The evaluation metric, $AUROC_n$, is the area under the roc curve for the n^{th} left-out evaluation fold in a three-fold cross-validation scheme. We then used TPE to randomly sample an initial uniform distribution of each of our hyperparameters and window sizes and evaluate the loss function for each random set of inputs. TPE then replaces this initial distribution with a new distribution built on the results from regions of the sampled distribution that minimize $L(x)$:

$$p(x | y) = \begin{cases} l(x) & \text{if } y < y^* \\ g(x) & \text{if } y \geq y^* \end{cases}$$

where y^* is a quantile γ of the observed y values so that $p(y < y^*) = \gamma$. Importantly, y^* is guaranteed to be greater than the minimum observed loss, so that some points are used to build $l(x)$. TPE then chooses candidate hyperparameters to sample as those representing the greatest expected improvement, EI , according to the expression:

$$EI_{y^*}(x) = \frac{\gamma y^* l(x) - l(x) \int_{-\infty}^{y^*} y p(y) dy}{y l(x) + (1 - \gamma) g(x)} \propto \left(\gamma + \frac{g(x)}{l(x)} (1 - \gamma) \right)^{-1}$$

To maximize EI , the algorithm picks points x with high probability under $l(x)$ and low probability under $g(x)$. Each iteration of the algorithm returns x^* , the next set of hyperparameters to sample, with the greatest EI based on previously sampled points.

Training the classifier. The ECLAIR classifier was trained in three stages, using a custom wrapper of the scikit-learn⁷³ random forest⁷⁴ classifier to allow for use of TPE to search both algorithm hyperparameters and residue window sizes simultaneously. In all cross-validations performed, we allowed TPE to search the following hyperparameters, beginning with uniform distributions of the indicated ranges: (i) minimum samples per leaf (0–1,000), (ii) maximum fraction of features per tree (0–1), and (iii) split criterion (entropy or gini diversity index). The number of estimators (decision trees) in each random forest was fixed at either 200 for training the feature selection classifiers or 500 for training the full ensemble. We also allowed TPE to search over residue window sizes (± 0 –5 residues for a total window of up to 11 residues, centered on the residue of interest). This was achieved by allowing extra features for neighboring residues to be included at the time of algorithm initialization.

In the first stage of training, cross-validation using TPE was performed on classifiers trained using only features from one of the five feature categories. The feature or set of features from each category with the minimum loss was selected to represent that category in building the ensemble classifier (**Supplementary Table 4**). In the second stage, the ensemble classifier was built of eight random forest classifiers, each trained on different subsets of feature categories, and hyperparameters and window sizes were again chosen using cross-validation and TPE (**Supplementary**

Table 5). In the final stage, following performance measurement on the testing set, the eight subclassifiers were retrained using the full set of 3,447 interactions with at least 50% UniProt residue coverage in the PDB, using the same hyperparameters and window sizes found in the previous step.

Evaluating the ensemble. After training and optimizing using only the training set, we predicted interface residues in a completely orthogonal testing set. For each subclassifier of the ensemble, all residues in the testing set that could be predicted (given the full set of necessary features or a superset) were ranked according to their raw prediction scores to produce ROC and precision–recall plots.

Benchmarking against other methods. Interfaces for interactions in our testing set were computed using several popular interface prediction methods^{20–24}. We compiled a set of representative protein structures from the PDB for each protein in our testing set, selecting the structure with the highest UniProt residue content based on SIFTS and excluding any PDB structures of interacting protein pairs from our testing set. We then evaluated the precision, recall, and false positive rate for proteins that were able to be classified by all methods. These represent point estimates of these metrics for the external methods with binary prediction scores.

We also compared ECLAIR with ten popular methods for interface prediction by predicting interfaces in a standard benchmark set of protein complexes²⁵ (**Supplementary Table 1**). Here, we followed the experimental procedures laid out by Maheshwari *et al.*²⁶ and excluded complexes in which the receptor is <50 or >600 amino acids, where the interface is made up of <20 residues, or where multiple interfaces are present.

Predicting new interfaces. We retrained the ensemble using all available cocrystal structures, including those from both testing and training sets, a standard machine learning practice that makes maximum use of labeled data⁷⁵. Using this fully trained ensemble of classifiers, we predicted interface residues for the remaining 185,957 interactions not resolved by either PDB structures or homology models. Subclassifiers were ordered based on the number and information content of features used in their training. Each residue was then predicted by only the top-ranking classifier of the ensemble trained on the full set or a subset of available features for that residue.

Interface enrichment and three-dimensional atomic clustering. Interface domain enrichment, residue enrichment, and 3D atomic clustering can be calculated through the Interactome INSIDER web interface. For enrichments presented in this study, we accessed all disease mutations from the Human Gene Mutation Database (HGMD)²⁸ and ClinVar²⁹, recurrent cancer mutations appearing ≥6 times in COSMIC³⁰, and population variants from the Exome Sequencing Project³¹ to compute the log odds ratio:

$$LOR = \ln \left(\frac{\frac{p_1}{1-p_1}}{\frac{p_2}{1-p_2}} \right)$$

where p_1 is the probability of a mutation or variant being at the interface, and p_2 is the probability of any residue being at the interface. We computed the log odds ratio for residues in each of the interface prediction potential categories. We also computed the log odds ratio for interactions with known interfaces from PDB cocrystal structures, defined as all known interface residues from NACCESS calculations and all residues in Pfam⁷⁶ domains with ≥5 interface residues. For the disease mutation enrichment analysis (**Fig. 4a**), we used all disease mutations available from HGMD, and the following numbers of mutations occurred in each category: 10,196 very low; 10,547 low; 2,970 medium; 1,135 high; and 305 very high. We also computed enrichment of 18,638 mutations in known interfaces and 17,760 mutations in known noninterfaces (from cocrystal structure evidence).

To perform 3D atomic clustering of amino acid loci of interest, we used an established method³⁵ for clustering and empirical P value calculation and applied it to multiprotein clustering, wherein clusters can occur across an interaction interface. Here, we perform complete-linkage clustering⁷⁷ in the shared 3D space of both proteins, and iteratively, and randomly rearrange mutations in each protein to produce an empirical null distribution of cluster sizes.

Mutagenesis validation experiments. We performed mutagenesis experiments in which we introduced random human population variants from the Exome Sequencing Project³¹ into known and predicted interfaces. We randomly selected mutations of predicted interface residues in each of the top four ECLAIR categories (low–very high). As positive and negative controls, we also selected random mutations of known interface and noninterface residues in cocrystal structures in the PDB. The selected mutations were then introduced into the proteins according to our previously published Clone-seq pipeline²⁷, and their impact (either disrupting or maintaining the interaction) was assessed using our yeast two-hybrid assay (**Supplementary Note 7**). In this manner, we tested the impact of 2,164 mutations: 1,664 in our predicted interfaces and 500 in known interface and noninterface residues from cocrystal structures. In **Figure 2c**, we report the fraction of tested interface residue mutations that caused a disruption of the given interaction for each of the interface residue bins.

Web server. Interactome INSIDER is deployed as an interactive web server (<http://interactomeinsider.yulab.org>) containing known and predicted interfaces for 198,503 protein interactions in eight species as well as variants and functional annotations mapped relative to the residues in the human proteome. For each interaction, the most reliable, high-resolution model is presented—i.e., cocrystal structures are always displayed in lieu of homology models, and all remaining unresolved interactions are predicted by our ECLAIR classifier. Cocrystal structures are derived from the PDB, with extraneous chains removed for each interaction, and homology models are computed by MODELLER¹¹ and downloaded from Interactome3D¹². For both types of structural model, we computed all residues at the interface over all available models and allow users to view any model from which a unique interface residue has been calculated. For predicted interfaces, a nonredundant set of single-protein models are shown when available, with locations of predicted interface residues indicated. In total, the resource contains 7,135

interactions with cocrystal structures, 5,411 with homology models, and 185,957 with predicted interfaces.

Interactome INSIDER also includes precalculated enrichment of mutations derived from several sources: 56,159 disease mutations from HGMD²⁸ and ClinVar²⁹ and 1,300,352 somatic cancer mutations from COSMIC³⁰. It also includes 194,396 population variants from the 1000 Genomes Project³², 425,115 from the Exome Sequencing Project³¹, and 54,165 catalogued by UniProt³³. Predictions of deleteriousness for all variants and any user-submitted variants within the curated interactomes are obtained from PolyPhen-2 (ref. 36) and SIFT⁷⁸, and biophysical property change guides (i.e., polar to nonpolar, hydrophobic to hydrophilic) are also displayed for convenience. Mutation and variant-enrichment analyses can be triggered by the user for existing variants or for user-submitted sets within interacting protein domains, residues, and 3D clustering using the atomic coordinates of structures when available.

Downloads of known and predicted interface residues on a per-interaction basis are available as plain text and as .bed files that can be visualized alongside other genomic landmarks in the UCSC genome browser⁷⁹. Per-protein visualization tracks, with interface residues of all interaction partners, are also available on the “Downloads” page, along with bulk downloads of interfaces for entire species.

Statistics. Statistical analyses were performed using a two-sided *Z* test or a two-sided Mann–Whitney *U* test, as indicated in the figure captions. Exact *P* values are provided for all compared groups, and comparisons with a two-sided *P* value < 0.05 are considered significant, with all others considered not significant (n.s.).

Code availability. Custom code used in this study is freely available at <https://github.com/hyulab/ECLAIR> and as **Supplementary Software**.

Life Sciences Reporting Summary. Further information regarding the experimental design may be found in the **Life Sciences Reporting Summary**.

Data availability. Data produced by this study is available for browsing and bulk download at <http://interactomeinsider.yulab.org>. Source data for **Figures 1, 2, 4 and 5** are available online.

56. Orchard, S. *et al.* Protein interaction data curation: the International Molecular Exchange (IMEx) consortium. *Nat. Methods* **9**, 345–350 (2012).
57. Salwinski, L. *et al.* The Database of Interacting Proteins: 2004 update. *Nucleic Acids Res.* **32**, D449–D451 (2004).
58. Kerrien, S. *et al.* The IntAct molecular interaction database in 2012. *Nucleic Acids Res.* **40**, D841–D846 (2012).
59. Licata, L. *et al.* MINT, the molecular interaction database: 2012 update. *Nucleic Acids Res.* **40**, D857–D861 (2012).
60. Chatr-Aryamontri, A. *et al.* The BioGRID interaction database: 2015 update. *Nucleic Acids Res.* **43**, D470–D478 (2015).
61. Turner, B. *et al.* iRefWeb: interactive analysis of consolidated protein interaction data and their supporting evidence. *Database (Oxford)* **2010**, baq023 (2010).
62. Keshava Prasad, T.S. *et al.* Human Protein Reference Database--2009 update. *Nucleic Acids Res.* **37**, D767–D772 (2009).
63. Mewes, H.W. *et al.* MIPS: curated databases and comprehensive secondary data resources in 2010. *Nucleic Acids Res.* **39**, D220–D224 (2011).
64. Alfano, C. *et al.* The Biomolecular Interaction Network Database and related tools 2005 update. *Nucleic Acids Res.* **33**, D418–D424 (2005).
65. Ruepp, A. *et al.* CORUM: the comprehensive resource of mammalian protein complexes--2009. *Nucleic Acids Res.* **38**, D497–D501 (2010).
66. Güldener, U. *et al.* MPact: the MIPS protein interaction resource on yeast. *Nucleic Acids Res.* **34**, D436–D441 (2006).
67. Brown, K.R. & Jurisica, I. Online predicted human interaction database. *Bioinformatics* **21**, 2076–2082 (2005).
68. Pagel, P. *et al.* The MIPS mammalian protein-protein interaction database. *Bioinformatics* **21**, 832–834 (2005).
69. Hermjakob, H. *et al.* The HUP0 PSI's molecular interaction format--a community standard for the representation of protein interaction data. *Nat. Biotechnol.* **22**, 177–183 (2004).
70. Berman, H.M. *et al.* The Protein Data Bank. *Nucleic Acids Res.* **28**, 235–242 (2000).
71. Velankar, S. *et al.* SIFTS: Structure Integration with Function, Taxonomy and Sequences resource. *Nucleic Acids Res.* **41**, D483–D489 (2013).
72. Lee, B. & Richards, F.M. The interpretation of protein structures: estimation of static accessibility. *J. Mol. Biol.* **55**, 379–400 (1971).
73. Pedregosa, F. *et al.* Scikit-learn: machine learning in Python. *J. Mach. Learn. Res.* **12**, 2825–2830 (2011).
74. Breiman, L. Random forests. *Mach. Learn.* **45**, 5–32 (2001).
75. Witten, I.H., Frank, E., Hall, M.A. & Pal, C.J. *Data Mining: Practical Machine Learning Tools and Techniques* (Elsevier Science, 2016).
76. Punta, M. *et al.* The Pfam protein families database. *Nucleic Acids Res.* **40**, D290–D301 (2012).
77. Sørensen, T. A method of establishing groups of equal amplitude in plant sociology based on similarity of species and its application to analyses of the vegetation on Danish commons. *Biol. Skr.* **5**, 1–34 (1948).
78. Kumar, P., Henikoff, S. & Ng, P.C. Predicting the effects of coding non-synonymous variants on protein function using the SIFT algorithm. *Nat. Protoc.* **4**, 1073–1081 (2009).
79. Tyner, C. *et al.* The UCSC Genome Browser database: 2017 update. *Nucleic Acids Res.* **45** D1, D626–D634 (2017).

Life Sciences Reporting Summary

Nature Research wishes to improve the reproducibility of the work that we publish. This form is intended for publication with all accepted life science papers and provides structure for consistency and transparency in reporting. Every life science submission will use this form; some list items might not apply to an individual manuscript, but all fields must be completed for clarity.

For further information on the points included in this form, see [Reporting Life Sciences Research](#). For further information on Nature Research policies, including our [data availability policy](#), see [Authors & Referees](#) and the [Editorial Policy Checklist](#).

▶ Experimental design

1. Sample size

Describe how sample size was determined.

Sample sizes were chosen based on data availability or independent benchmarks.

2. Data exclusions

Describe any data exclusions.

No data were excluded from analyses.

3. Replication

Describe whether the experimental findings were reliably reproduced.

N/A -- only bulk experiments performed, with trends derived from many individuals.

4. Randomization

Describe how samples/organisms/participants were allocated into experimental groups.

Interactions were allocated into groups according to an independent benchmark set or availability of machine learning features.

5. Blinding

Describe whether the investigators were blinded to group allocation during data collection and/or analysis.

Data blinding present in experimental data collection, up until creation of final figures for mutagenesis experiment. Data blinding is used as is typical in machine learning, with test-set folds left out during algorithm training.

Note: all studies involving animals and/or human research participants must disclose whether blinding and randomization were used.

6. Statistical parameters

For all figures and tables that use statistical methods, confirm that the following items are present in relevant figure legends (or in the Methods section if additional space is needed).

n/a Confirmed

- The exact sample size (n) for each experimental group/condition, given as a discrete number and unit of measurement (animals, litters, cultures, etc.)
- A description of how samples were collected, noting whether measurements were taken from distinct samples or whether the same sample was measured repeatedly
- A statement indicating how many times each experiment was replicated
- The statistical test(s) used and whether they are one- or two-sided (note: only common tests should be described solely by name; more complex techniques should be described in the Methods section)
- A description of any assumptions or corrections, such as an adjustment for multiple comparisons
- The test results (e.g. P values) given as exact values whenever possible and with confidence intervals noted
- A clear description of statistics including central tendency (e.g. median, mean) and variation (e.g. standard deviation, interquartile range)
- Clearly defined error bars

See the web collection on [statistics for biologists](#) for further resources and guidance.

► Software

Policy information about [availability of computer code](#)

7. Software

Describe the software used to analyze the data in this study.

Custom software was used, and is available for download via github (<https://github.com/hyulab/ECLAIR>).

For manuscripts utilizing custom algorithms or software that are central to the paper but not yet described in the published literature, software must be made available to editors and reviewers upon request. We strongly encourage code deposition in a community repository (e.g. GitHub). *Nature Methods* [guidance for providing algorithms and software for publication](#) provides further information on this topic.

► Materials and reagents

Policy information about [availability of materials](#)

8. Materials availability

Indicate whether there are restrictions on availability of unique materials or if these materials are only available for distribution by a for-profit company.

There are no restrictions on experimental materials. ORF clones used in yeast two-hybrid assays are available upon request.

9. Antibodies

Describe the antibodies used and how they were validated for use in the system under study (i.e. assay and species).

N/A

10. Eukaryotic cell lines

a. State the source of each eukaryotic cell line used.

N/A

b. Describe the method of cell line authentication used.

N/A

c. Report whether the cell lines were tested for mycoplasma contamination.

N/A

d. If any of the cell lines used are listed in the database of commonly misidentified cell lines maintained by [ICLAC](#), provide a scientific rationale for their use.

N/A

► Animals and human research participants

Policy information about [studies involving animals](#); when reporting animal research, follow the [ARRIVE guidelines](#)

11. Description of research animals

Provide details on animals and/or animal-derived materials used in the study.

N/A

Policy information about [studies involving human research participants](#)

12. Description of human research participants

Describe the covariate-relevant population characteristics of the human research participants.

N/A